Commun. Comput. Phys.
doi: 10.4208/cicp.010113.160813s

Vol. **15**, No. 4, pp. 996-1011
April 2014

Exponential Runge-Kutta Methods for the Multispecies Boltzmann Equation

Qin Li[1] and Xu Yang[2]*

[1] *Department of Mathematics, University of Wisconsin, Madison, WI 53706, USA.*
[2] *Department of Mathematics, University of California, Santa Barbara, CA 93106-3080, USA.*

Received 1 January 2013; Accepted (in revised version) 16 August 2013

Available online 21 January 2014

Abstract. This paper generalizes the exponential Runge-Kutta asymptotic preserving (AP) method developed in [G. Dimarco and L. Pareschi, *SIAM Numer. Anal.*, 49 (2011), pp. 2057–2077] to compute the multi-species Boltzmann equation. Compared to the single species Boltzmann equation that the method was originally applied on, this set of equation presents a new difficulty that comes from the lack of local conservation laws due to the interaction between different species. Hence extra stiff nonlinear source terms need to be treated properly to maintain the accuracy and the AP property. The method we propose does not contain any nonlinear nonlocal implicit solver, and can capture the hydrodynamic limit with time step and mesh size independent of the Knudsen number. We prove the positivity and strong AP properties of the scheme, which are verified by two numerical examples.

AMS subject classifications: 65C20, 65M06, 76D05, 82C40

Key words: Multispecies Boltzmann equation, exponential Runge-Kutta method, hydrodynamic limit, asymptotic preserving property, positivity preserving.

1 Introduction

We are interested in developing efficient numerical methods for the nonlinear multispecies Boltzmann equation [11]:

$$\partial_t f_i + v\cdot\nabla_x f_i = \frac{1}{\varepsilon}Q_i(f,f), \quad t\geq 0, \quad (x,v)\in\mathbb{R}^d\times\mathbb{R}^d. \tag{1.1}$$

*Corresponding author. *Email addresses:* qinli@caltech.edu (Q. Li), xuyang@math.ucsb.edu (X. Yang)

Here $f_i(t,x,v)$ represents the distribution function of the i-th species at time t, position x and velocity v, and $f=(f_1,f_2,\cdots,f_N)^{\mathrm{T}}$, d is the dimensionality and N is the number of species. The collision term is given by

$$Q_i(f,f)=\sum_{k=1}^{N}Q_{ik}(f,f), \tag{1.2a}$$

$$\begin{aligned}Q_{ik}(f,f)(v)&=\int_{S^{d-1}}\int_{\mathbb{R}^d}(f_i'f_{k^*}'-f_if_{k^*})B_{ik}(|v-v_*|,\omega)dv_*d\omega\\&\triangleq Q_{ik}^{+}-f_iQ_{ik}^{-},\end{aligned} \tag{1.2b}$$

where B_{ik} is the symmetric collision kernel (*i.e.* $B_{ik}=B_{ki}$), v and v_* are pre-collisional velocities, v' and v_*' are post-collisional velocities, $f_i'=f_i(t,x,v')$ and $f_{k^*}'=f_k(t,x,v_*')$, ω is a unit vector, and S^{d-1} is the unit sphere defined in $\mathbb{R}^d$ space, $g=v-v_*$ is relative velocity. There are many variations for the collision kernel B_{ik}. One of the simple cases is the Maxwell molecule when $B_{ik}=B_{ik}\left(\frac{g\cdot\omega}{|g|}\right)$. The post-collisional velocities v' and v_*' satisfy:

$$v'=v-\frac{\mu_{ik}}{m_i}(g-|g|\omega),\qquad v_*'=v_*+\frac{\mu_{ik}}{m_k}(g-|g|\omega), \tag{1.3}$$

with $\mu_{ik}=\frac{m_im_k}{m_i+m_k}$ being the reduced mass, and m_i, m_k being the mass for species i and k respectively. This deduction is based on momentum and energy conservations:

$$m_iv+m_kv_*=m_iv'+m_kv_*',\qquad m_i|v|^2+m_k|v_*|^2=m_i|v'|^2+m_k|v_*'|^2.$$

Eq. (1.1) describes the evolution of rarefied gas that has more than two components whose particles usually have different masses. It is often used in modeling the high altitude gas, which is usually considered as a binary mixture of Oxygen and Nitrogen, and the environment at the reentry to the earth of spacecrafts. In (1.2b), the gaining part is marked as Q_{ik}^{+} and the rest is the losing part marked as $f_iQ_{ik}^{-}$ with f_i extracted out of the integration. In (1.1), the ε is called the Knudsen number, indicating the ratio of mean free path over the typical domain size. When $\varepsilon=\mathcal{O}(1)$, the equation is in kinetic (microscopic) regime. As $\varepsilon\to 0$, one gets to fluid (macroscopic) regime with the Euler equations as the first order approximation in Chapman-Enskog Expansion [**?**].

Numerical challenge comes from the time discretization due to the Knudsen number. On the one hand, it is impractical to design an implicit method since it requires the inversion of the nonlocal and nonlinear collision term. On the other hand, if explicit method is used, the time step is limited by the smallest Knudsen number for stability reasons, which usually leads to unaffordable computational cost.

There has been a great amount of literature on removing the numerical stiffness in (1.1), many of which are based on domain decomposition [5, 8, 9, 16, 18, 25–27]. The idea is to solve (1.1) when the Knudsen number is of $\mathcal{O}(1)$, and to solve its Euler limit when the Knudsen number is small. Despite its success in theory, the method encounters two difficulties in practice: 1. It is hard to identify how small the Knudsen number should

be so that the Euler limit is a good approximation, hence the boundary that separates the two domains is not clear; 2. Given the boundary, the coupling condition of the two systems can not be easily derived (*e.g.* [2–4]).

An alternative approach, that we are going to pursue in this paper, is called the asymptotic preserving (AP) method [21, 22]. It looks for fast and simple solvers for the Boltzmann equation in all ranges of Knudsen number. When the Knudsen number gets small, it automatically captures its macroscopic asymptotic limits without refining the mesh. Compared to the multi-physics domain decomposition methods, this framework only solves the microscopic equations, and thus avoids the complexity introduced by switching back and forth to the macroscopic equations. There are several variations of AP property, including weakly-AP, relaxed-AP, and strongly-AP defined respectively as follows, given small ε:

- *Weakly-AP*. If the data are within $\mathcal{O}(\varepsilon)$ of the local equilibrium initially, they remain so for all future time steps;
- *Relaxed-AP*. For non-equilibrium initial data, the solution will be projected to the local equilibrium beyond an initial layer (after several time steps);
- *Strongly-AP*. For non-equilibrium initial data, the solution will be projected to the local equilibrium immediately in one time step.

In general, the strongly-AP property is preferred, and is the designing principle for most of the classical AP schemes [6, 20]. The relaxed-AP is a concept introduced recently in [12], which was shown numerically sufficient in capturing the hydrodynamic limit. The weakly-AP is often a necessary condition for the AP property. We refer to [12] for more details.

Recently several AP methods are generated for the single species system. Based on the fact that BGK operator is a good approximation to the collision term, Filbet and Jin proposed a BGK penalization method [12]. It writes the collision term as a summation of the BGK approximation, which is stiff and treated implicitly, and a remainder term, which is not stiff and computed explicitly. The method enjoys two benefits: it is an AP scheme and thus the time step is relaxed; although the BGK operator is treated implicitly, there exists an explicit way to compute it [7]. Another major AP method was developed by Pareschi and Dimarco in [10]. They used the time splitting method, and during the collision step, they wrote the equation in an exponential way so that under mild conditions on the Runge-Kutta (RK) method, the distribution function is forced to the equilibrium numerically, which captures the asymptotic limit. This method was generalized in [29] later on, where the time splitting was avoided so that the RK method could be applied to the entire equation, and the numerical accuracy can reach up to an arbitrary order. Other AP methods, *e.g.* the Wild Sum and micro-macro decomposition method, can be found in [15] and [28] respectively.

However, one encounters essential difficulties in extending these AP methods to the multi-species system (1.1). Since the species exchange momentum and energy [17,19], the

conservation laws break down for each single species, and the associated macroscopic quantities are hard to be obtained. Therefore it is hard to compute the local Maxwellian, which the aforementioned AP methods highly rely on. In fact, the collision term (1.2) is nonlinear and of $\mathcal{O}(\varepsilon^{-1})$, which brings up difficulties in computation. Besides that, theoretically, species should gradually share the common velocity and common temperature as time evolves. Hence, to prove the AP property of numerical methods for multi-species system, it is no longer enough to only prove the convergence to the equilibrium, which is usually the case for the single species system.

In order to overcome these difficulties, we develop an exponential Runge-Kutta (Exp-RK) method where a newly defined unified Maxwellian is embedded instead of the local Maxwellian used in [10]. It reduces the complexity in the computation of the local Maxwellian, while preserves the correct asymptotic limit. Compared to [23] where relaxed-AP is achieved, this method is strongly AP, hence only one time step is needed for arbitrary initial data to be projected to the unified Maxwellian. Moreover, it preserves the positivity of the distribution function, which is usually hard for high-order accurate schemes to maintain.

The rest of the paper is organized as follows. In Section 2, we briefly introduce the properties of the multi-species Boltzmann equation. The numerical method will be described in details in Section 3, with the analysis of its properties given in Section 4. We present two numerical examples to show the performance of the method in Section 5, and make conclusive remarks in Section 6.

2 Properties of the multi-species Boltzmann equation

In this section, we briefly introduce the macroscopic quantities, conserved quantities, and the Euler limit of the multi-species Boltzmann equation (1.1).

2.1 Macroscopic quantities and conservation

For the i-th species, the number density n_i, the mass density ρ_i, the average velocity u_i, the total energy E_i, the specific internal energy e_i, the temperature T_i, the stress tensor S_i, and the heat flux vector q_i are defined by

$$n_i=\int f_i \mathrm{d}v, \qquad \rho_i=m_i n_i, \qquad \rho_i u_i=m_i\int v f_i \mathrm{d}v, \tag{2.1a}$$

$$E_i=\frac{1}{2}\rho_i u_i^2+n_i e_i=\frac{1}{2}m_i\int |v|^2 f_i \mathrm{d}v, \qquad e_i=\frac{d}{2}T_i=\frac{m_i}{2n_i}\int f_i|v-u_i|^2\mathrm{d}v, \tag{2.1b}$$

$$S_i=\int (v-u_i)\otimes(v-u_i) f_i \mathrm{d}v, \qquad q_i=\frac{1}{2}m_i\int (v-u_i)|v-u_i|^2 f_i \mathrm{d}v. \tag{2.1c}$$

The total mass density ρ, the total number density n, the mean velocity $\bar{u}$, the total energy E, the internal energy $n\bar{e}$ and the mean temperature $\bar{T}$ are defined by

$$\rho=\sum_i \rho_i, \qquad n=\sum_i n_i, \qquad \rho\bar{u}=\sum_i \rho_i u_i, \tag{2.2a}$$

$$E=\sum_i E_i = n\bar{e}+\frac{1}{2}\rho|\bar{u}|^2, \qquad \bar{T}=\frac{2\bar{e}}{d}. \tag{2.2b}$$

Eq. (1.1) implies, for each species, the mass is conserved, but not the momentum and energy. On the other hand, the total momentum and energy is conserved. This means

$$\int m_i Q_i \mathrm{d}v=\sum_i \int m_i v_i Q_i \mathrm{d}v=\sum_i \int \frac{1}{2} m_i v_i^2 Q_i \mathrm{d}v=0. \tag{2.3}$$

2.2 The Euler limit

When the system reaches the local equilibrium, the gaining part balances the losing part, *i.e.* $Q_i(f)=0$ for each i. Therefore, by [1],

$$f_i=\overline{M}_i=n_i\left(\frac{m_i}{2\pi\bar{T}}\right)^{d/2}\exp\left(-\frac{m_i|v-\bar{u}|^2}{2\bar{T}}\right), \tag{2.4}$$

where $\bar{T}$ and $\bar{u}$ are defined in (2.2). (2.4) is called the unified Maxwellian because $\bar{u}$ and $\bar{T}$ are given by the quantities of the entire system instead of each single species. This is different from the local Maxwellian where the velocity and temperature is used for each species.

With (2.4), the first order Chapman-Enskog expansion gives the Euler limit for the multi-species system [1],

$$\partial_t \rho_i+\nabla_x\cdot(\rho_i\bar{u})=0, \tag{2.5a}$$

$$\partial_t(\rho\bar{u})+\nabla_x\cdot(\rho\bar{u}\otimes\bar{u}+n\bar{T}\boldsymbol{I})=0, \tag{2.5b}$$

$$\partial_t E+\nabla_x\cdot((E+n\bar{T})\bar{u})=0, \tag{2.5c}$$

where $\boldsymbol{I}$ is the identity matrix. Note that in (2.5a), the advection term is $\rho_i\bar{u}$ instead of $\rho_i u_i$, since $u_i\to\bar{u}$ and $T_i\to\bar{T}$ as $\varepsilon\to 0$.

3 Exponential Runge-Kutta method

We systematically introduce the Exponential Runge-Kutta (Exp-RK) method to solve (1.1) in this section. The algorithm consists of two parts for each time step:

Step 1. Solve the convection part,

$$\partial_t f_i+v\cdot\nabla_x f_i=0. \tag{3.1}$$

Step 2. Solve the collision part,

$$\partial_t f_i = \frac{Q_i}{\varepsilon}. \tag{3.2}$$

This is based on the Strang splitting algorithm, and thus the accuracy is second order in time. The details of the numerical solvers for the two parts are shown below. Here we only consider $d=1$, and leave the high-dimensional case for future study since it is technically more involved.

3.1 Convection part

We use the upwind scheme with the van Leer limiter to compute (3.1):

$$f_i^{l+\frac{1}{2}} = f_i^l - \Delta t v \cdot \nabla_x f_i^l, \tag{3.3}$$

where Δt is the time step. The flux term for the i-th species at grid point x_j is discretized as:

$$v\partial_x f_{i,j} = \nu(f_{i,j_1} - f_{i,j_1-1}) - \frac{\Delta x}{2}\nu\big(\mathrm{sgn}(\nu)-\nu\big)(\sigma_{i,j_1} - \sigma_{i,j_1-1}), \tag{3.4}$$

where the index i stands for the i-th species, and the indexes j and j_1 are for mesh grids.

In (3.4), $\nu = v/\Delta x$, with Δx being the mesh size. $j_1 = j$ for $v>0$, $j_1 = j+1$ for $v<0$, and

$$\sigma_{i,j} = \frac{f_{i,j+1}-f_{i,j}}{\Delta x}\phi_{i,j}, \qquad \phi(\theta) = \frac{\theta+|\theta|}{\theta+1}, \qquad \theta_{i,j} = \frac{f_{i,j}-f_{i,j-1}}{f_{i,j+1}-f_{i,j}}. \tag{3.5}$$

3.2 Collision part

Since (3.2) is a stiff equation, the time step in explicit methods is limited by ε, while implicit method has difficulties in directly inverting Q. In order to overcome these difficulties, one could use the Exp-RK method, and the idea is to reformulate (3.2) into the exponential form, and then solve it by the Runge-Kutta scheme.

3.2.1 Reformulation

Define

$$\mu = \text{constant} > \sup_{x,i}|Q_i^-|, \qquad P_i = Q_i + \mu f_i, \tag{3.6}$$

and rewrite (3.2) as:

$$\begin{aligned}\partial_t\big((f_i-\overline{M}_i)e^{\mu t/\varepsilon}\big) &= \partial_t f_i e^{\mu t/\varepsilon} + (f_i-\overline{M}_i)\frac{\mu}{\varepsilon}e^{\mu t/\varepsilon} = \frac{1}{\varepsilon}(Q_i+\mu f_i-\mu\overline{M}_i)e^{\mu t/\varepsilon}\\ &= \frac{1}{\varepsilon}(P_i-\mu\overline{M}_i)e^{\mu t/\varepsilon},\end{aligned} \tag{3.7}$$

in which we have used the fact that $\mathrm{d}\overline{M}_i/\mathrm{d}t = 0$ since ρ_i, $\bar{u}$ and $\bar{T}$ do not change in the collision step.

Remark 3.1. 1. Eq. (3.7) describes the evolution of the difference between the distribution function f_i and its equilibrium $\overline{M}_i$ multiplied by an integration factor, and thus removes the stiffness in (3.2) [10].

2. Eq. (3.7) holds for an arbitrary constant μ. The way we choose μ is to guarantee the positivity of P; we refer to [29] for more details.

3.2.2 Runge-Kutta method

Applying the K-stage Runge-Kutta method to Eq. (3.7) gives

$$\begin{cases} \text{Stage } \alpha\text{:} & (f^{l,(\alpha)}-\overline{M})e^{\frac{\mu}{\varepsilon}c_\alpha\Delta t}=(f^{l+\frac{1}{2}}-\overline{M})+\dfrac{\Delta t}{\varepsilon}\displaystyle\sum_{\beta=1}^{\alpha-1}a_{\alpha\beta}(P^{l,(\beta)}-\mu\overline{M})e^{\frac{\mu}{\varepsilon}c_\beta\Delta t}, \\ \text{Final stage:} & (f^{l+1}-\overline{M})e^{\frac{\mu}{\varepsilon}\Delta t}=(f^{l+\frac{1}{2}}-\overline{M})+\dfrac{\Delta t}{\varepsilon}\displaystyle\sum_{\alpha=1}^{K}b_\alpha(P^{l,(\alpha)}-\mu\overline{M})e^{\frac{\mu}{\varepsilon}c_\alpha\Delta t}, \end{cases} \tag{3.8}$$

where $\sum_{\beta=1}^{\alpha-1}a_{\alpha\beta}=c_\alpha$, $\sum_\alpha b_\alpha=1$, and $Y^{l,(\beta)}$ stands for the estimate of Y at $t=t_l+c_\beta\Delta t$. The last equation implies

$$f^{l+1}=\left(1-e^\lambda-\sum_\alpha b_\alpha\lambda e^{\lambda(-1+c_\alpha)}\right)\overline{M}+e^{-\lambda}f^{l+\frac{1}{2}}+\sum_\alpha b_\alpha\lambda e^{\lambda(c_\alpha-1)}\frac{P^{l,(\alpha)}}{\mu},\quad \lambda=\frac{\mu h}{\varepsilon}, \tag{3.9}$$

where μ is given in (3.6), and $f^{l+\frac{1}{2}}$ is obtained in (3.3). In this formulation, one needs to compute $\overline{M}$ and P, both of which will be discussed in details below.

3.2.3 Computation of $\overline{M}$

To get $\overline{M}$ defined in (2.4), we only need to compute the following quantities

$$n_i^{l+1}=n_i^{l+1/2}=n_i^l-\Delta t\int v\cdot\nabla_x f_i^l\,\mathrm{d}v, \tag{3.10a}$$

$$(\rho\bar{u})^{l+1}=(\rho\bar{u})^{l+1/2}=(\rho\bar{u})^l-\Delta t\sum_i m_i\int v\otimes v\cdot\nabla_x f_i^l\,\mathrm{d}v, \tag{3.10b}$$

$$E^{l+1}=E^{l+1/2}=E^l-\Delta t\sum_i\int\frac{m_i}{2}|v|^2v\cdot\nabla_x f_i^l\,\mathrm{d}v, \tag{3.10c}$$

$$\bar{T}^{l+1}=\bar{T}^{n+1/2}=\frac{2E^{l+1}-(\rho\bar{u}^2)^{l+1}}{n^{l+1}}, \tag{3.10d}$$

where the computation for the flux term is given in (3.4). The first equalities are due to the invariance of these quantities in the collision step.

3.2.4 Evaluation of P

Since $P=Q+\mu f$, we only need to show the computation of the collision term Q. The spectral method for computing the collision term Q was first developed in [14, 30], and

the fast version that reduces the computational cost to $N\log_2(N)$ was found later on in [13]. However, those schemes are mainly for the single-species systems, but in our case, the system has more than one species. Due to the mass difference, the collision term loses many symmetries, and thus the fast version could be easily carried through. We follow the method introduced in [23] using the basic spectral method, and leave the designing of the fast algorithm to further studies.

We use a ball $B(0,S)$ to represent the domain, out of which f is negligible. We periodize f on $v\in[-L,L]^d$ with $L\geq(3+\sqrt{2})S$. L is chosen much larger than S to avoid non-physical collision at different periods of the periodized f. Define the Fourier and inverse Fourier transforms as:

$$\hat{f}(p)=\int f(v)e^{-\mathrm{i}p\cdot v}\mathrm{d}v,\qquad f(v)=\frac{1}{(2L)^d}\sum_p\hat{f}(p)e^{\mathrm{i}p\cdot v}, \tag{3.11}$$

where $\mathrm{i}=\sqrt{-1}$ is the imaginary unit. Then Q_{ik}^+ in (1.2b) becomes

$$Q_{ik}^+=\frac{1}{(2L)^{2d}}\sum_{p,q}\hat{f}_i(p)\hat{f}_k(q)e^{\mathrm{i}(p+q)\cdot v}\int\!\!\int B_{ik}e^{\mathrm{i}\eta\cdot g+\mathrm{i}|g|\gamma\cdot\omega}\mathrm{d}v_*\mathrm{d}\omega, \tag{3.12}$$

where

$$\eta=\frac{-m_k}{m_i+m_k}p+\frac{-m_k}{m_i+m_k}q,\qquad \gamma=\frac{m_k}{m_i+m_k}p-\frac{m_i}{m_i+m_k}q.$$

Particularly, when B_{ik} is a constant (for Maxwell molecule),

$$v'=\frac{m_i-m_k}{m_i+m_k}v+\frac{2m_k}{m_i+m_k}v_*,\qquad v'_*=\frac{2m_i}{m_i+m_k}v-\frac{m_i-m_k}{m_i+m_k}v_*.$$

Then (3.12) becomes

$$Q_{ik}^+=\frac{B_{ik}}{(2L)^2}\sum_{p,q}\hat{f}_i(p)\hat{f}_k(q)e^{\mathrm{i}\left(\frac{m_i-m_k}{m_i+m_k}p+\frac{2m_i}{m_i+m_k}q\right)v}\int e^{\mathrm{i}\left(\frac{2m_k}{m_i+m_k}p-\frac{m_i-m_k}{m_i+m_k}q\right)v_*}\mathrm{d}v_*.$$

Therefore

$$\begin{aligned}\hat{Q}_{ik}^+(r)&=\frac{B_{ik}}{(2L)^2}\sum_{p,q}\hat{f}_i(p)\hat{f}_k(q)\int e^{\mathrm{i}\left(\frac{m_i-m_k}{m_i+m_k}p+\frac{2m_i}{m_i+m_k}q-r\right)v}\mathrm{d}v\int e^{\mathrm{i}\left(\frac{2m_k}{m_i+m_k}p-\frac{m_i-m_k}{m_i+m_k}q\right)v_*}\mathrm{d}v_*\\&=B_{ik}\sum_{p,q}\hat{f}_i(p)\hat{f}_k(q)\mathrm{sinc}(\mathrm{a})\mathrm{sinc}(\mathrm{b}),\end{aligned}$$

where

$$a=\left(\frac{m_i-m_k}{m_i+m_k}p+\frac{2m_i}{m_i+m_k}q-r\right)L,\qquad b=\left(\frac{2m_k}{m_i+m_k}p-\frac{m_i-m_k}{m_i+m_k}q\right)L.$$

One can use FFT to compute $\hat{f}_i(p)$ and $\hat{f}_k(q)$, and get Q_{ik} by the inverse FFT.

The computation for $f_iQ_{ik}^-$ is much simpler,

$$f_iQ_{ik}^-=f_i\int B_{ik}f_k\mathrm{d}v_k=f_in_kB_{ik}. \tag{3.13}$$

Altogether, $Q_i=\sum_kQ_{ik}$.

4 Positivity and asymptotic preserving properties

In this section, we discuss the positivity and asymptotic preserving properties of the Exp-RK method introduced in Section 3.

Theorem 4.1 (Positivity)**.** *The Exp-RK method described by* (3.3) *and* (3.8) *preserves the positivity property of f_i, i.e. there exist $h_*>0$ and $\mu_*>0$ such that $f^{l+1}>0$ provided $f^l>0$, if $0<\Delta x<h_*$ in* (3.3) *and $\mu>\mu_*$ in* (3.8)*.*

The proof of Theorem 4.1 is essentially the same as in [29, Theorem 1], and we omit the details here.

In order to prove the AP property, we need the following assumption:

Assumption 1. The operator P satisfies

$$\|P(f,f)-P(g,g)\|\lesssim\|f-g\|.$$

Remark that this assumption is true for Maxwell molecule in the d_2 norm defined in $P_s(\mathbb{R}^d)$ space ([31]). This can be easily seen by a similar argument that one of the authors did in [29, Appendix].

Assume f^l and g^l are the initial conditions to (3.8). Define

$$\begin{aligned}&d_0=\left\|f^l-g^l\right\|,\qquad d_\alpha=\left\|f^{l,(\alpha)}-g^{l,(\alpha)}\right\|,\quad \alpha=1,\cdots,K,\\&\vec{d}=(d_1,d_2,\cdots,d_K)^{\mathrm{T}},\qquad \vec{b}=(b_1,b_2,\cdots,b_K)^{\mathrm{T}},\qquad \vec{e}=(1,1,\cdots,1)^{\mathrm{T}},\end{aligned}$$

and $\boldsymbol{A}$ is a $K\times K$ strictly lower triangular matrix and $\boldsymbol{E}$ is a diagonal matrix given by

$$\boldsymbol{A}_{\alpha\beta}=\frac{\lambda}{\mu}a_{\alpha\beta}e^{(c_\beta-c_\alpha)\lambda},\quad \beta<\alpha,\quad \text{and}\quad \boldsymbol{E}=\mathrm{diag}\{e^{-c_1\lambda},e^{-c_2\lambda},\cdots,e^{-c_K\lambda}\},\tag{4.1}$$

where $a_{\alpha\beta}$, b_α and c_α are the coefficients of the Runge-Kutta method in (3.8), λ is given in (3.9) and $\vec{e}$ is a K-dimensional vector. Note that $\boldsymbol{A}$ is strictly lower triangular as the Runge-Kutta method we use is explicit. Then we have the following contraction lemma.

Lemma 4.1. *After one time step iteration in* (3.8)*, the scheme satisfies:*

$$\left\|f^{l+1}-g^{l+1}\right\|\le R(\lambda)\left\|f^{l+\frac{1}{2}}-g^{l+\frac{1}{2}}\right\|\tag{4.2a}$$

with

$$R(\lambda)=e^{-\lambda}\left(1+\frac{C\lambda}{\mu}\vec{b}^{\mathrm{T}}\boldsymbol{E}^{-1}(\boldsymbol{I}-C\boldsymbol{A})^{-1}\boldsymbol{E}\vec{e}\right),\tag{4.2b}$$

where $\boldsymbol{I}$ is the identity matrix, and $C>0$ is a constant.

Proof. Eq. (3.8) implies, for $\alpha=1,\cdots,K$,

$$(f^{l,(\alpha)}-g^{l,(\alpha)})e^{c_\alpha\lambda}=(f^{l+\frac{1}{2}}-g^{l+\frac{1}{2}})+\sum_{\beta=1}^{\alpha-1}a_{\alpha\beta}\frac{\lambda}{\mu}e^{c_\beta\lambda}\left(P_f^{l,(\beta)}-P_g^{l,(\beta)}\right). \tag{4.3}$$

Using the triangle inequality and Assumption 1 produces

$$\left\|f^{l,(\alpha)}-g^{l,(\alpha)}\right\|\le\left\|f^{l+\frac{1}{2}}-g^{l+\frac{1}{2}}\right\|e^{-c_\alpha\lambda}+\sum_{\beta=1}^{\alpha-1}a_{\alpha\beta}\frac{\lambda}{\mu}e^{(c_\beta-c_\alpha)\lambda}\left(C\left\|f^{l,(\beta)}-g^{l,(\beta)}\right\|\right), \tag{4.4}$$

which implies

$$\vec{d}\le d_0\boldsymbol{E}\vec{e}+C\boldsymbol{A}\vec{d}\quad\text{and}\quad\vec{d}\le d_0(\boldsymbol{I}-C\boldsymbol{A})^{-1}\boldsymbol{E}\vec{e}, \tag{4.5}$$

where we have used the fact that $\boldsymbol{A}$ is a strictly lower triangular matrix.

The final step in (3.8) yields

$$\left(f^{l+1}-g^{l+1}\right)=\left(f^{l+\frac{1}{2}}-g^{l+\frac{1}{2}}\right)e^{-\lambda}+\sum_{\alpha=1}^{K}\frac{hb_\alpha}{\varepsilon}\left(P_f^{l,(\alpha)}-P_g^{l,(\alpha)}\right)e^{(c_\alpha-1)\lambda}. \tag{4.6}$$

Then (4.5) and Assumption 1 imply

$$\left\|f^{l+1}-g^{l+1}\right\|\le d_0e^{-\lambda}+\frac{C\lambda}{\mu}e^{-\lambda}\vec{b}^{\mathrm{T}}\boldsymbol{E}^{-1}\vec{d}\le d_0e^{-\lambda}\left(1+\frac{C\lambda}{\mu}\vec{b}^{\mathrm{T}}\boldsymbol{E}^{-1}(\boldsymbol{I}-C\boldsymbol{A})^{-1}\boldsymbol{E}\vec{e}\right), \tag{4.7}$$

which completes the proof. □

Lemma 4.2. *Under Assumption 1,* $\left\|f^l-\overline{M}^l\right\|=\mathcal{O}\left(R(\lambda)\right)$ *for each l.*

Proof. Take $g=\overline{M}$ in (4.2) yields

$$\left\|f^{l+1}-\overline{M}^{l+1}\right\|\le\left\|f^{l+\frac{1}{2}}-\overline{M}^{l+\frac{1}{2}}\right\|R(\lambda).$$

By (3.3) and (3.10), one has

$$\left\|f^{l+\frac{1}{2}}-\overline{M}^{l+\frac{1}{2}}\right\|<\left\|f^l-\overline{M}^l\right\|+\Delta t\left\|v\cdot\nabla_x\left(f^l-M^l\right)\right\|\le\left\|f^l-\overline{M}^l\right\|+\mathcal{O}(\Delta t).$$

The above two inequalities imply the conclusion. □

Theorem 4.2. *The Exp-RK method defined in* (3.3) *and* (3.8) *is strong AP.*

Proof. By Lemma 4.2, it suffices to prove that $R(\lambda)=\mathcal{O}(\varepsilon)$ for small ε. Considering that $\boldsymbol{A}$ is a strictly lower triangular matrix and is thus a nilpotent, one has

$$\boldsymbol{E}^{-1}(\boldsymbol{I}-\boldsymbol{A})^{-1}\boldsymbol{E}=\boldsymbol{E}^{-1}\left(\boldsymbol{I}+\boldsymbol{A}+\boldsymbol{A}^2+\cdots+\boldsymbol{A}^{K-1}\right)\boldsymbol{E}=\boldsymbol{I}+\boldsymbol{B}+\boldsymbol{B}^2+\cdots+\boldsymbol{B}^{K-1}, \tag{4.8}$$

where $\boldsymbol{B}=\boldsymbol{E}^{-1}\boldsymbol{A}\boldsymbol{E}$, and we have used $\boldsymbol{A}^K=0$. Further by (4.1), $\boldsymbol{B}_{\alpha\beta}=\boldsymbol{A}_{\alpha\beta}e^{c_\alpha\lambda-c_\beta\lambda}=\frac{\lambda}{\mu}a_{\alpha\beta}$. Thus $\boldsymbol{I}+\sum_\alpha \boldsymbol{B}^\alpha$ is a matrix with the elements of at most $\mathcal{O}(\lambda^K)$. Therefore, when $\varepsilon\ll 1$,

$$R(\lambda)=e^{-\lambda}\left(1+\frac{C\lambda}{\mu}\vec{b}\cdot\boldsymbol{E}^{-1}(\boldsymbol{I}-\boldsymbol{A})^{-1}\boldsymbol{E}\cdot\vec{e}\right)=\mathcal{O}(e^{-\lambda}\lambda^K)<\mathcal{O}(\varepsilon).$$

This completes the proof. □

Remark 4.1. Note that in the derivation for (3.7), the only requirement on $\overline{M}$ is that it does not change with respect to time in the collision part. Analytically, one can replace this $\overline{M}$ by arbitrary function that does not has the time variable. However, the associated numerics simply can not preserve the right asymptotic limit, as indicated in Lemma 4.2.

5 Numerical examples

We take the examples in [23, 24] for the convenience of comparisons. The BGK penalization method for multi-species Boltzmann equation can be found in [12]. When ε is big, we compute the reference solution using the forward Euler method with very small time step and mesh size. For small ε, we directly compute the solution to the Euler equation as the reference solution.

Example 5.1 (A Stationary Shock)**.** We consider the two species model, *i.e.* $N=2$ in (1.1). We choose the initial data for the macroscopic quantities so that a shock with zero speed would form in its Euler limit:

$$\begin{cases} m_1=1,\ m_2=1.5,\ n_1=n_2=1,\ u_1=1.8,\ u_2=1.3,\ T_1=T_2=0.325, & \text{if } x<0,\\ m_1=1,\ m_2=1.5,\ n_1=n_2=1.401869,\ u_1=u_2=1.07,\ T_1=T_2=0.8605, & \text{if } x>0. \end{cases}$$

The initial conditions for the distribution is chosen to be far away from the Maxwellian:

$$f_i(t=0,x,v)=\sum_{\ell=1}^{2}A_{i,\ell}\exp\left(-B_{i,\ell}(v-C_{i,\ell})^2\right),\qquad i=1,2,$$

where

$$B_{i,\ell}=\frac{\rho_i}{4E_i-2\rho_i u_i^2(1+\kappa^2)},\quad A_{i,\ell}=\frac{n_i}{2}\sqrt{\frac{B_{i,\ell}}{\pi}},\quad C_{i,1}-u_i=u_i-C_{i,2}=\kappa u_i,\quad \kappa=0.2.$$

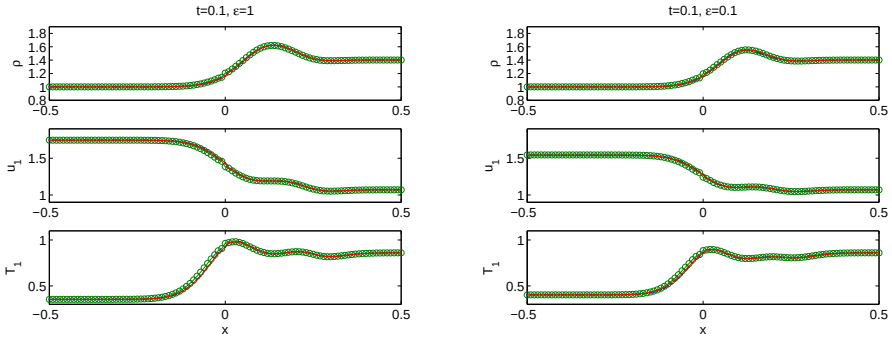

Figure 1: Example 5.1, we compare the numerical results at $t=0.1$ by the Exp-RK method (the dotted line), the BGK penalization method (the circled line), and the reference solution (the solid line). The left figures are for $\varepsilon=1$, and the right ones are for $\varepsilon=0.1$.

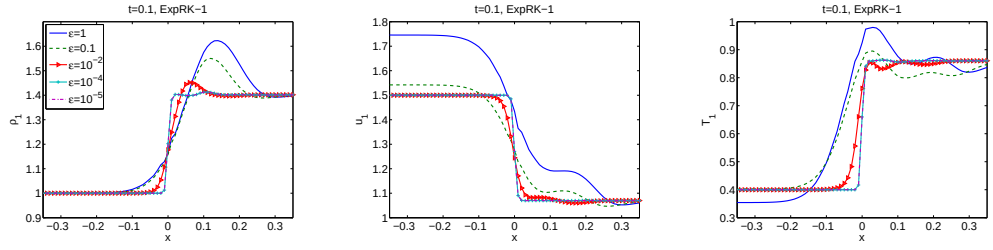

Figure 2: Example 5.1, as ε goes to zero, the results get to the Euler limit, *i.e.* a stationary shock.

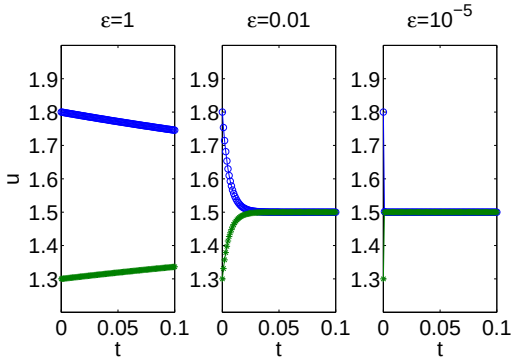

Figure 3: Example 5.1, the velocities converge to the mean velocity at different rates for different ε at $x=-1$. The circles and stars stand for the velocities of the first and second species respectively. The smaller ε gives the faster convergence rate.

We choose $\Delta t=0.0005$ and $\Delta x=0.01$. In Fig. 1, we compare the numerical results given by the Exp-RK method, the BGK penalization method, and the reference solution for $\varepsilon=1$ and 0.1. In Fig. 2, we verify the AP property of the Exp-RK method, *i.e.* as ε goes to zero, the numerical results capture the stationary shock. We compare the convergence of the velocities for two species in Fig. 3, where they gradually converge to the mean velocity u, and the smaller ε gives the faster convergence rate.

Example 5.2 (A Sod Problem)**.** The macroscopic quantities are taken as

$$\begin{cases} m_1=m_2=1,\ n_1=1,\ n_2=1.2,\ u_1=0.6,\ u_2=-0.5,\ T_1=T_2=0.709, & \text{if } x<0,\\ m_1=m_2=1,\ n_1=0.125,\ n_2=0.2,\ u_1=-0.2,\ u_2=0.125,\ T_1=T_2=0.075, & \text{if } x>0. \end{cases}$$

The initial conditions for f_i, $i=1,2$ are

$$f_i(t=0,x,v)=\sum_{\ell=1}^{2} A_{i,\ell}\exp\left(-B_{i,\ell}(v-C_{i,\ell})^2\right),$$

where

$$B_{i,\ell}=\frac{\rho_i}{4E_i-2\rho_i u_i^2(1+\kappa^2)},\quad A_{i,\ell}=\frac{n_i}{2}\sqrt{\frac{B_{i,\ell}}{\pi}},\quad C_{i,1}-u_i=u_i-C_{i,2}=\kappa u_i,\quad \kappa=0.2.$$

In this example, the two species have the same mass, therefore the results of computing this system as a mixture of two species should agree with those of a single species system. We take $\Delta t=0.001$ and $\Delta x=0.01$. We show this indistinguishability in Fig. 4. In

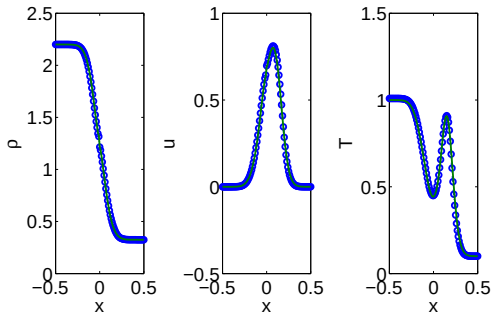

Figure 4: Example 5.2, indistinguishability. The solid lines are the results of treating the system as single species, and they agree with the results given by the dashed lines, which are the results of a system that has two species with the same mass.

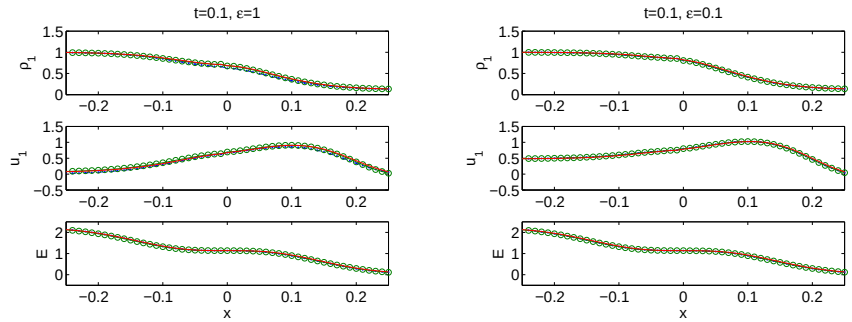

Figure 5: Example 5.2, at $t=0.1$, we compare the results give by the Exp-RK method (the dotted line), the BGK penalization method (the circled line) and the reference solution (the solid line). The left figures are for $\varepsilon=1$, and the right ones are for $\varepsilon=0.1$.

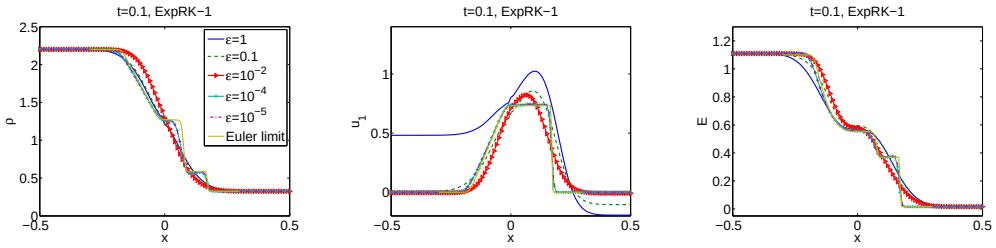

Figure 6: Example 5.2, as ε goes to zero, the numerical results by the Exp-RK method converge to the Euler limit.

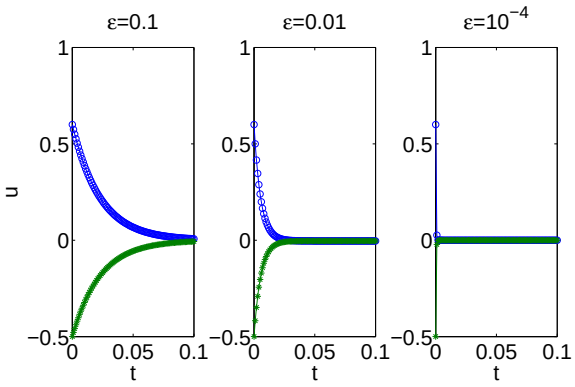

Figure 7: Example 5.2, the velocities converge to the mean velocity at different rates for different ε at $x=-1$. The circled line stands for species one, and the dotted line stands for species two. The smaller ε gives the faster convergence rate.

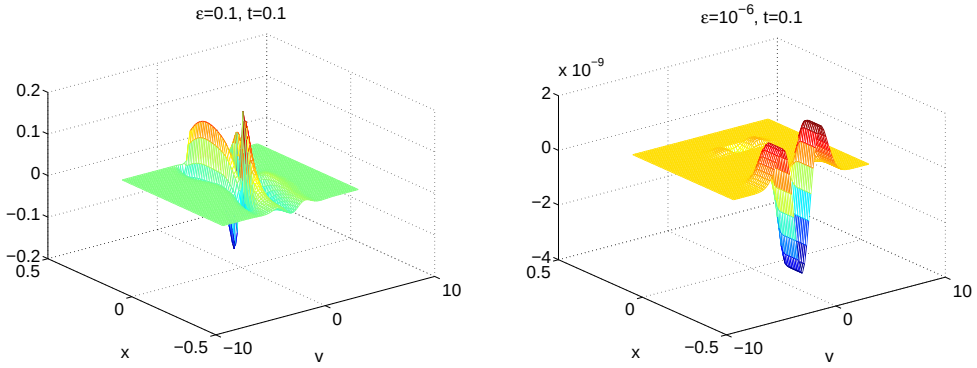

Figure 8: Example 5.2, $f-M$ for $\varepsilon=1$ and $\varepsilon=10^{-6}$ at $t=0.1$.

Fig. 5, we compare the numerical results of the Exp-RK method to those of the BGK penalization method and the reference solution for $\varepsilon=1$ and 0.1. In Fig. 6, we verify the AP property by taking $\varepsilon\to 0$. As one can see, the numerical results capture the corresponding Euler limit. In Fig. 7, we show that in the long time limit, the two species have the same velocity, and the smaller ε gives the faster convergence rate. We show the difference between f and local Maxwellian M at $t=0.1$ for $\varepsilon=10^{-6}$ in Fig. 8.

6 Conclusion

In this paper, we generalized the Exp-RK method in [10] to compute the multi-species Boltzmann equation. Compared to the single species Boltzmann equation that was originally studies in [10], we need to embed the unified Maxwellian to the method in order to overcome the difficulties from the lack of local conservation laws, which is due to the interaction between different species. The method we propose does not contain any nonlinear nonlocal implicit solver, and we prove it is strongly AP and preserves the positivity, which is usually hard for high-order accurate schemes to maintain. The numerical examples presented here are only in one dimension, and we leave the case of higher dimension for future study since it is technically more involved.

Acknowledgments

Q.L. was partially supported by the NSF grant DMS-1114546 and NSF Research Network in Mathematical Sciences "KI-Net: Kinetic description of emerging challenges in multiscale problems of natural sciences". X.Y. was partially supported by the startup funding of University of California, Santa Barbara.

References

[1] P. Andries, K. Aoki, and B. Perthame, A consistent BGK-type model for gas mixtures, J. Stat. Phys., 106 (2002), pp. 993–1018.
[2] C. Bardos, F. Golse, and Y. Sone, Half-space problems for the boltzmann equation: A survey, J. Stat. Phys., 124 (2006), pp. 275–300.
[3] C. Besse, S. Borghol, T. Goudon, I. Lacroix-Violet, and J.-P. Dudon, Hydrodynamic regimes, Knudsen layer, numerical schemes: Definition of boundary fluxes, Adv. Appl. Math. Mech., 3 (2011), pp. 519–561.
[4] A. Bobylev, R. Grzhibovskis, and A. Heintz, Entropy inequalities for evaporation/condensation problem in rarefied gas dynamics, J. Stat. Phys., 102 (2001), pp. 1151–1176.
[5] J. Bourgat, P. Le Tallec, B. Perthame, and Y. Qiu, Coupling Boltzmann and Euler equations without overlapping, in Domain Decomposition Methods in Science and Engineering, A. Quarteroni, J. Périaux, Y. A. Kuznetsov, and O. Widlund, eds., Providence, RI, 1994, AMS, pp. 377–398.
[6] R. Caflisch, S. Jin, and G. Russo, Uniformly accurate schemes for hyperbolic systems with relaxations, SIAM J. Numer. Anal., 34 (1997), pp. 246–281.
[7] F. Coron and B. Perthame, Numerical passage from kinetic to fluid equations, SIAM J. Numer. Anal., 28 (1991), pp. 26–42.
[8] P. Degond and S. Jin, A smooth transition model between kinetic and diffusion equations, SIAM J. Numer. Anal., 42 (2005), pp. 2671–2687.
[9] P. Degond, S. Jin, and L. Mieussens, A smooth transition model between kinetic and hydrodynamic equations, J. Comput. Phys., 209 (2005), pp. 665–694.
[10] G. Dimarco and L. Pareschi, Exponential Runge–Kutta methods for stiff kinetic equations, SIAM J. Numer. Anal., 49 (2011), pp. 2057–2077.

[11] J. H. Ferziger and H. G. Kaper, Mathematical Theory of Transport Processes in Gases, North-Holland Pub. Co, 1972.
[12] F. Filbet and S. Jin, A class of asymptotic-preserving schemes for kinetic equations and related problems with stiff sources, J. Comput. Phys., 229 (2010), pp. 7625–7648.
[13] F. Filbet, C. Mouhot, and L. Pareschi, Solving the Boltzmann equation in N log2N, SIAM J. Sci. Comput., 28 (2006), pp. 1029–1053.
[14] F. Filbet and G. Russo, High order numerical methods for the space non homogeneous Boltzmann equation, J. Comput. Phys, 186 (2003), pp. 457–480.
[15] E. Gabetta, L. Pareschi, and G. Toscani, Relaxation schemes for nonlinear kinetic equations, SIAM J. Numer. Anal, 34 (1997), pp. 2168–2194.
[16] F. Golse, S. Jin, and C. D. Levermore, A domain decomposition analysis for a two-scale linear transport problem, Math. Model Num. Anal, 37 (2002), pp. 869–892.
[17] H. Grad, in Rarefied Gas Dynamics, F. Devienne, ed., Pergamon, London, England, 1960, pp. 10–138.
[18] M. Guenther, J. Struckmeier, P. Le Tallec, and J. Perlat, Numerical modeling of gas flows in the transition between rarefied and continuum regimes, Notes on Numerical Fluid Mechanics, 66 (1998), pp. 222–241.
[19] B. B. Hamel, Kinetic model for binary gas mixtures, Physics of Fluids, 8 (1965), pp. 418–425.
[20] S. Jin, Runge-Kutta methods for hyperbolic conservation laws with stiff relaxation terms, J. Comput. Phys., 122 (1995), pp. 51–67.
[21] S. Jin, Efficient asymptotic-preserving (AP) schemes for some multiscale kinetic equations, SIAM J. Sci. Comput., 21 (1999), pp. 441–454.
[22] S. Jin, Asymptotic preserving (AP) schemes for multiscale kinetic and hyperbolic equations: a review, Lecture Notes for Summer School on "Methods and Models of Kinetic Theory" (M&MKT), Porto Ercole (Grosseto, Italy), June 2010.
[23] S. Jin and Q. Li, A BGK-penalization-based asymptotic-preserving scheme for the multispecies Boltzmann equation, Numer. Methods Partial Differential Equations, (2012).
[24] S. Jin and Y. Shi, A micro-macro decomposition-based asymptotic-preserving scheme for the multispecies Boltzmann equation, SIAM J. Sci. Comput., 31 (2010), pp. 4580–4606.
[25] S. Jin, X. Yang, and G. Yuan, A domain decomposition method for a two-scale transport equation with energy flux conserved at the interface, Kinet. Relat. Models, 1 (2008), pp. 65–84.
[26] A. Klar, H. Neunzert, and J. Struckmeier, Transition from kinetic theory to macroscopic fluid equations: A problem for domain decomposition and a source for new algorithms, Transport Theory Statist. Phys., 29 (2000), pp. 93–106.
[27] P. Le Tallec and F. Mallinger, Coupling Boltzmann and Navier-Stokes equations by half fluxes, J. Comput. Phys., 136 (1997), pp. 51–67.
[28] M. Lemou and L. Mieussens, A new asymptotic preserving scheme based on micro-macro formulation for linear kinetic equations in the diffusion limit, SIAM J. Sci. Comput., 31 (2008), pp. 334–368.
[29] Q. Li and L. Pareschi, Exponential Runge-Kutta schemes for inhomogeneous Boltzmann equations with high order of accuracy, arXiv:1208.2622.
[30] L. Pareschi and G. Russo, Numerical solution of the Boltzmann equation I: Spectrally accurate approximation of the collision operator, SIAM J. Numer. Anal, 37 (2000), pp. 1217–1245.
[31] G. Toscani and C. Villani, Probability metrics and uniqueness of the solution to the Boltzmann equation for a Maxwell gas, J. Stat. Phys., 94 (1999), pp. 619–637.